Micro and Nano Systems Letters

CORRESPONDENCE

Open Access

Highly stretchable multimodal sensor with split-line structural design for adaptive robotic grippers

Chan Hwa Hong[1], Sae Rom Seo[1], Min-Seok Kim[2], Young Kyu Hong[3], Min Hyung Kang[3] and Hye Jin Kim[1,4*]

Abstract

A large-area multimodal sensor device integrating pressure, temperature, humidity, proximity, and bending sensors was developed on a stretchable and flexible substrate. The substrate combines rigid polyimide with a soft elastomer to enhance stretchability, achieving up to 127% elongation through split-line structural designs that effectively relieve stress concentration. After 1,000 stretch-release cycles at 30% strain, resistance variation remained below 0.48%, confirming excellent mechanical durability. The pressure sensors exhibited high sensitivities of 27.5 kPa^{-1} (8-channel array) and 9.2 kPa^{-1} (18-channel array) across a wide pressure range, demonstrating suitability for robotic gripper applications. The central sensing units accurately measured bending (R^2 = 0.998), environmental parameters, and object distance with verified functionality. Overall, the device exhibits robust, reliable, and highly stretchable multimodal sensing performance, offering strong potential for advanced robotic manipulation and environmental monitoring applications.

Highlights

- A split-line patterned stretchable substrate was developed to mitigate slimming and crack formation, achieving 127% elongation, over threefold improvement compared with conventional designs.
- The integrated multimodal sensor platform (pressure, bending, temperature/humidity, proximity) maintained stable sensitivity and electrical continuity under 30% strain and 10^3 stretch cycles.
- The simple layout-level split-line strategy enables mechanically robust and wafer-compatible fabrication of next-generation adaptive robotic e-skin systems.

Keywords Stretchable substrate, Split-line, Slimming-reduction, Multimodal sensor, Robotic gripper

Introduction

Robotic manipulation increasingly relies on grippers capable of not only exerting appropriate forces but also perceiving contact state, object properties, and nearby obstacles in real time—driving a transition from single-channel touch to multimodal perception at the end-effector [1–6]. Recent demonstrations show that fusing tactile information with complementary modalities (e.g., temperature, proximity, bending/shape, slip) or with vision significantly enhances grasp stability and task success in unstructured environments [1–3, 7–10]. Empirically, autonomous soft-robotic systems equipped with distributed multimodal sensors have achieved self-adaptive manipulation and robust control policies across diverse objects, highlighting the value of sensor fusion at the gripper interface [1, 2].

*Correspondence:
Hye Jin Kim
nolawara@etri.re.kr

Full list of author information is available at the end of the article

Graphical Abstract

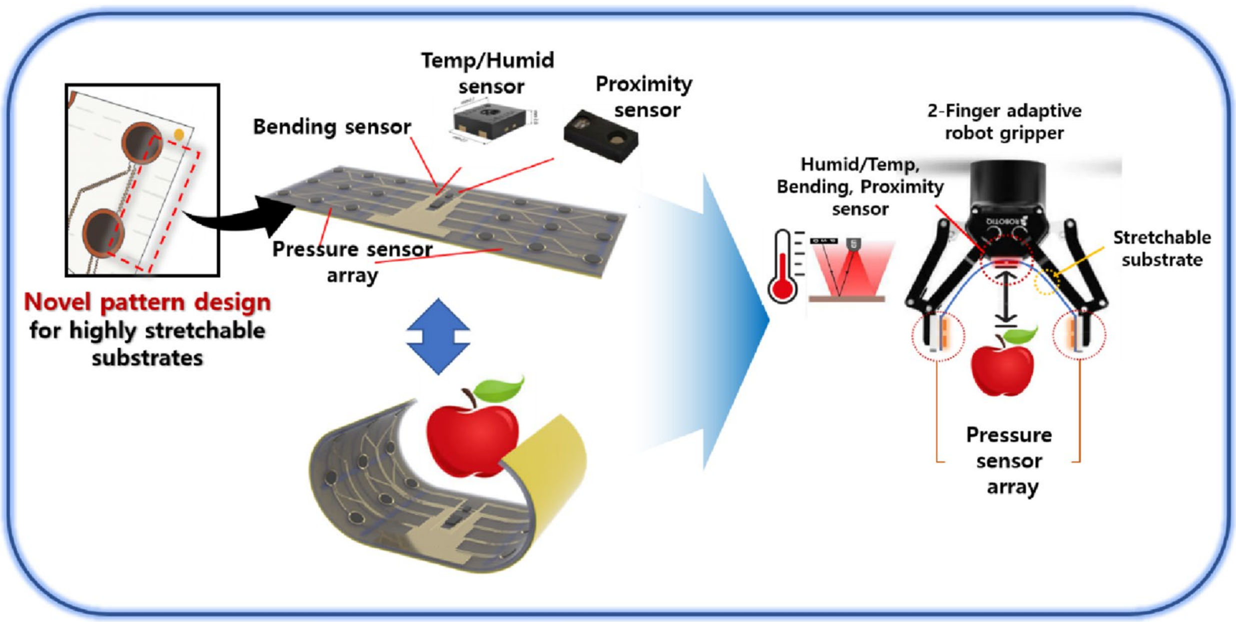

Despite this promise, systematic integration of heterogeneous sensors on grippers remains under-explored compared with vision-only or single-modality pipelines [7–12]. Canonical embedded-finger systems and continuum-robot arrays demonstrate the benefits of simultaneous force/pressure, proximity, acceleration, and temperature sensing, yet they also reveal persistent bottlenecks in substrate mechanics and packaging—limited conformability, repeated-deformation damage, long-term reliability—that impede scaling to deployable gripper skins [7–9, 11, 12]. To address these challenges, the field has increasingly adopted stretchable substrates and strain-engineered architectures including island–bridge layouts and kirigami-inspired cuts, which delocalize deformation, preserve electrical continuity under large cyclic strains, and maintain signal fidelity during shape change [13–21]. Mechanically, these approaches suppress strain localization and necking-induced thinning (geometric slimming)—precursors to microcracking and delamination in thin-film systems—by steering stresses through compliant bridges or patterned cuts [13–18]. Fundamentally, this geometric slimming is a manifestation of the Poisson effect, where longitudinal stretching induces a spontaneous transverse contraction of the elastomeric matrix. This phenomenon is characterized by an effective Poisson's ratio ($V_{eff} = -\epsilon_{trans}/\epsilon_{long}$); in conventional incompressible elastomers such as PDMS or Ecoflex, V approaches 0.5, leading to significant narrowing and thinning of the substrate under high strain [22]. Nevertheless, in highly elastic substrates, substantial elongation can still cause geometric slimming (a reduction in width/thickness accompanied by localized strain), amplifying local stress and triggering crack initiation or even tearing if not explicitly managed in the substrate layout. This phenomenon fundamentally limits allowable strain budgets and device lifetime for patterned conductors and stacked active layers, motivating explicit slimming-mitigation strategies in next-generation gripper skins [23].

To overcome these issues, we propose a novel "Split-line" structural design. The term "Split-line" is derived from the pattern's unique geometry, where the substrate layout diverges into multiple branches specifically at the regions where slimming is most prominent. This finger-like split configuration is strategically designed to suppress the transverse contraction (slimming) by effectively distributing the concentrated stress and decoupling the longitudinal strain from the transverse Poisson effect. Building on this substrate, we integrate a pressure-sensor array, temperature/humidity sensor, proximity (distance) sensor, and bending sensor into a single stretchable multimodal platform compatible with diverse robotic grippers. This combination of engineered stretchable substrates and multimodal sensing provides a practical route toward advanced robotic systems capable of dynamic and adaptive operation in complex, unstructured environments.

Materials and methods

Materials

Commercial glass wafers (EAGLE XG, Corning, USA) were used as the substrate for wafer-level fabrication. Metal electrodes were deposited by electron-beam evaporation using a Ti (10 nm)/Au (200 nm) bilayer structure. The polyimide (PI) films were prepared from PI-510 (Labotech, Korea) and subsequently cured under controlled vacuum conditions to achieve uniform thickness and mechanical flexibility. The elastomer layer employed for stretchable encapsulation and substrate transfer was Ecoflex 00–30 (HyupShin, Korea). For the fabrication of the conductive polymer composite, multi-walled carbon nanotubes (MWCNTs) were first dispersed in chloroform ($CHCl_3$) with poly(3-hexylthiophene) (P3HT) to ensure homogeneous dispersion and enhanced charge transport within the sensing layer. In the multimodal sensing platform, the proximity sensor chip (VCNL4040, Vishay, USA) and the temperature/humidity sensor chip (SHT4x series, Sensirion, Switzerland) were mounted onto the designated electrode pads using a soldering process. These components enabled integrated detection of proximity, temperature, and humidity within the flexible, stretchable substrate.

Design and fabrication

Figure 1 illustrates the conceptual design and operational principle of the multi-modal sensor system integrated into a two-finger robotic gripper. To enable intelligent perception and adaptive control during object manipulation, a stretchable multimodal sensor was developed and conformally attached to the inner surfaces of the gripper fingers. The sensor platform incorporates a pressure sensor array at the fingertip region for contact detection and force measurement, a bending sensor at the central area to monitor deformation and estimate object size, and temperature/humidity and proximity sensors to acquire environmental and positional information. When the robotic gripper approaches an object, the proximity sensor first detects its presence and measures the optimal approach distance. Once the object is within the grasping range, the control system commands the gripper to close its fingers. During contact, the pressure sensor array provides real-time tactile feedback, allowing the gripper to regulate the applied force and prevent slipping. The bending sensor quantifies the curvature induced by grasping, enabling estimation of object geometry and compliance. Meanwhile, the temperature and humidity sensors continuously monitor the ambient environment, enhancing the adaptability of the system to various conditions. The integrated sensing data are transmitted to the control unit, as represented in the right-hand graphs, which depict example outputs from each sensing module (pressure, bending, temperature, distance). These multimodal signals facilitate closed-loop feedback control and environmental awareness, enabling stable and intelligent manipulation of objects by the robotic system.

To mitigate slimming and mechanical failure of the stretchable multimodal sensor system under tensile strain, compliant interconnects were engineered in split-line motifs. Figure 2a shows two geometries: a bar-type split-line with dimensions 3.6×0.2 mm, and a tri-branch split-line whose total length is 3.6 mm, initial neck width is 0.2 mm, and terminal width expands to 0.8 mm through a three-way split; the branched segment (1.6 mm) occupies approximately 44% of the total length. The gap between neighboring split-lines is 2 mm. These compliant motifs redistribute local strain and thereby prevent crack initiation and tearing at high elongation, which is a key design element of this work. The overall device architecture is presented in Fig. 2b. Resistive pressure-sensor arrays are positioned at both gripping ends to measure normal contact forces, whereas the central region is reserved for heterogeneous integration

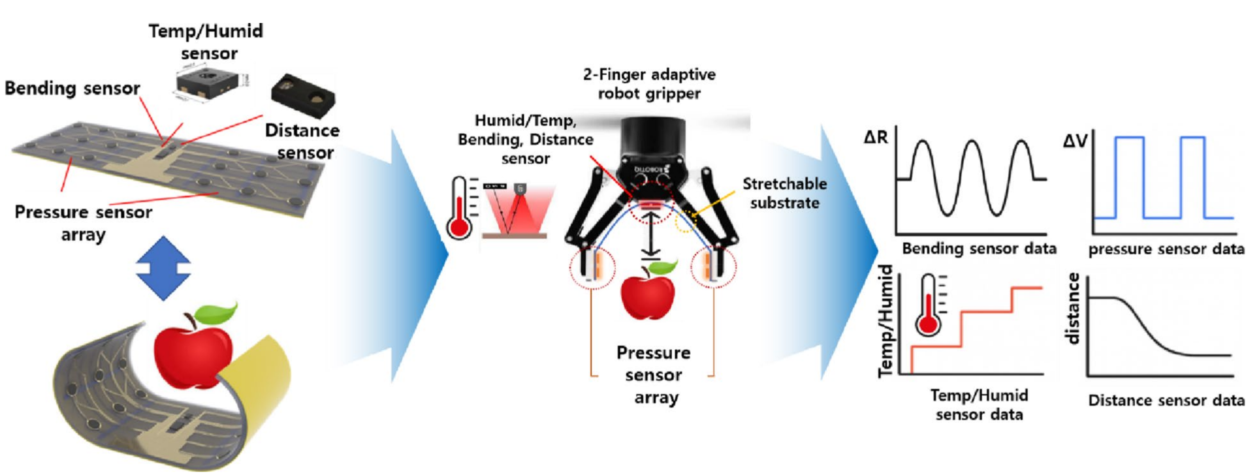

Fig. 1 Concept and operation of the stretchable multi-modal sensor system integrated into a two-finger robotic gripper

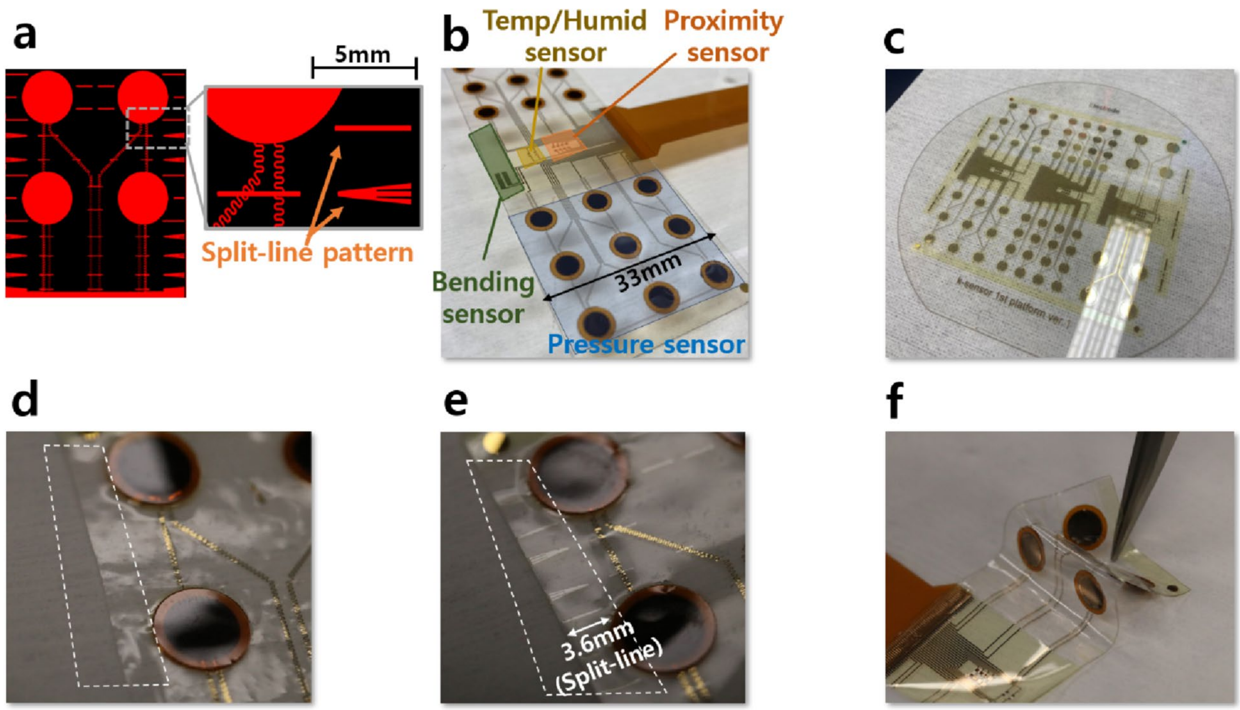

Fig. 2 Design and Photographs of the multimodal sensor array fabricated on the highly stretchable substrate. **a** Split-line structural design for mitigating slimming and mechanical failure under tensile strain. **b** Fabricated sensor photograph with resistive pressure arrays at both ends and provisions for integrating a bending sensor and multimodal digital chips (temperature/humidity and proximity sensors) at the center. **c** Wafer-level fabrication on a glass carrier using a PI/metal/PI layer with wet-processing. **d**-**e** Comparison of devices without and with split-lines, showing suppressed slimming and reduced cracking/tearing when split-lines are applied. **f** Elastomer transfer producing a soft, conformable, and stretchable laminate suitable for curved gripper surfaces

of a bending sensor and multimodal chips (temperature/humidity and proximity). This partitioning supports the entire manipulation workflow—from pre-grasp distance detection to grasp execution and in-grasp monitoring.

The wafer-level manufacturability is demonstrated in Fig. 2c. Three devices of approximately 33 × 100 mm are patterned on a 6-inch glass wafer using a PI/metal/PI structure (2 µm / 210 nm / 2 µm) formed via wet processes. Metal electrodes are deposited as Ti/Au = 10 nm / 200 nm, followed by PI patterning and curing at 320 °C in a vacuum oven for ~ 3 h. The devices are subsequently separated from the glass by 308 nm laser lift-off (LLO). The ultrathin wet processed PI affords excellent conformability on curved surfaces, which is advantageous for deployment on complex gripper geometries. The efficacy of the split-line design is contrasted in Fig. 2d and e. Without split-lines (Fig. 2d), straight interconnects exhibit pronounced edge thinning and local necking under strain. With split-lines (Fig. 2e), strain is dispersed by the compliant motifs, visibly suppressing slimming and reducing the propensity for cracking/tearing. Finally, Fig. 2f shows the soft, stretchable laminate obtained after transfer: following LLO, Ecoflex is poured and cured on a hotplate at 80 °C for ~ 3 h to form a PI/metal/PI–on–elastomer structure that maintains flexibility and high stretchability.

The pressure and bending sensors were designed based on a resistive sensing mechanism, in which the variation in the resistance of a conductive composite material reflects the magnitude of applied pressure or bending deformation. To fabricate these sensors, a solution-processable composite material was employed. The composite was primarily composed of a soft polymer matrix and a carbon-based conductive filler. Polyurethane (PU) was selected as the polymer matrix owing to its excellent processability for micro-patterning, high impact resistance, and superior mechanical durability. Multi-walled carbon nanotubes (MWCNTs) were adopted as the conductive filler due to their outstanding mechanical strength, thermal stability, high electrical conductivity, and compatibility with solution-based fabrication processes, which facilitate the formation of conductive polymer composites. For the preparation of the conductive composite, MWCNTs were first dispersed in chloroform with poly(3-hexylthiophene) and ultrasonically agitated for 5 h. The dispersion was then centrifuged at 8000 rpm for 30 min to obtain a homogeneous conductive solution. Subsequently, the prepared solution was mixed with polyurethane base resin and silver (Ag) particles, followed by additional ultrasonication for 1 h to ensure uniform dispersion. Finally, the resulting mixture was drop-cast onto a polyimide (PI) substrate using a droplet coating method to form the sensing layer for both pressure and bending sensors.

Results and discussion

Simulation and substrate characterization

To examine the mechanical role of the split-line design under tensile loading, we performed finite-element simulations using a device domain of 33 × 100 mm, consistent with the fabricated sensor. The regions accommodating the pressure sensor array and multimodal chips were modeled as rigid islands made of polyimide (PI), whereas the remaining sections were modeled as an elastomer to represent the stretchable substrate. This configuration allows comparison of strain evolution in the stretched region between adjacent rigid islands for designs with and without split-lines. Figure 3a shows the case without split-lines. Under 10% tensile strain, slimming initiates first in the soft elastomeric segments between rigid islands, indicating a necking-like deformation driven by local strain concentration. At 20% strain, this slimming becomes markedly more pronounced, forming narrow waists that bridge adjacent rigid islands. A closer view of the stretched part at 10% strain further reveals that the onset of slimming is centered between islands, where geometric discontinuities steer strain to accumulate. Such localized thinning implies elevated stress triaxiality, which substantially increases the likelihood of crack initiation and subsequent tearing during continued stretching. Figure 3b presents the design with split-lines inserted between rigid islands. While global slimming still develops under tensile loading, the maximum-thinning zones now coincide with the split-line motifs. The compliant paths provided by the split-lines redistribute local strain, effectively blunting the severity of slimming at these hot spots. As a result, the propensity for crack initiation is reduced, and the device is expected to sustain higher overall stretch before mechanical failure. Taken together, the simulations demonstrate that introducing split-lines mitigates necking in the inter-island ligaments, thereby lowering failure risk and enabling high-stretch operation without structural defects.

Figure 4a compares device deformation at 30% elongation for regions without and with split-lines on the same specimen. In the area lacking split-lines, pronounced slimming (necking) develops between the rigid pressure-sensor islands, indicating strong local strain concentration along straight interconnects (red line). In contrast, within the split-line region, the onset and severity of slimming are noticeably suppressed, consistent with the compliant paths that disperse tensile strain across the inter-island ligament (blue line). To further substantiate these observations, the supplementary figure (Figure S1) presents images of the devices under the same 30%

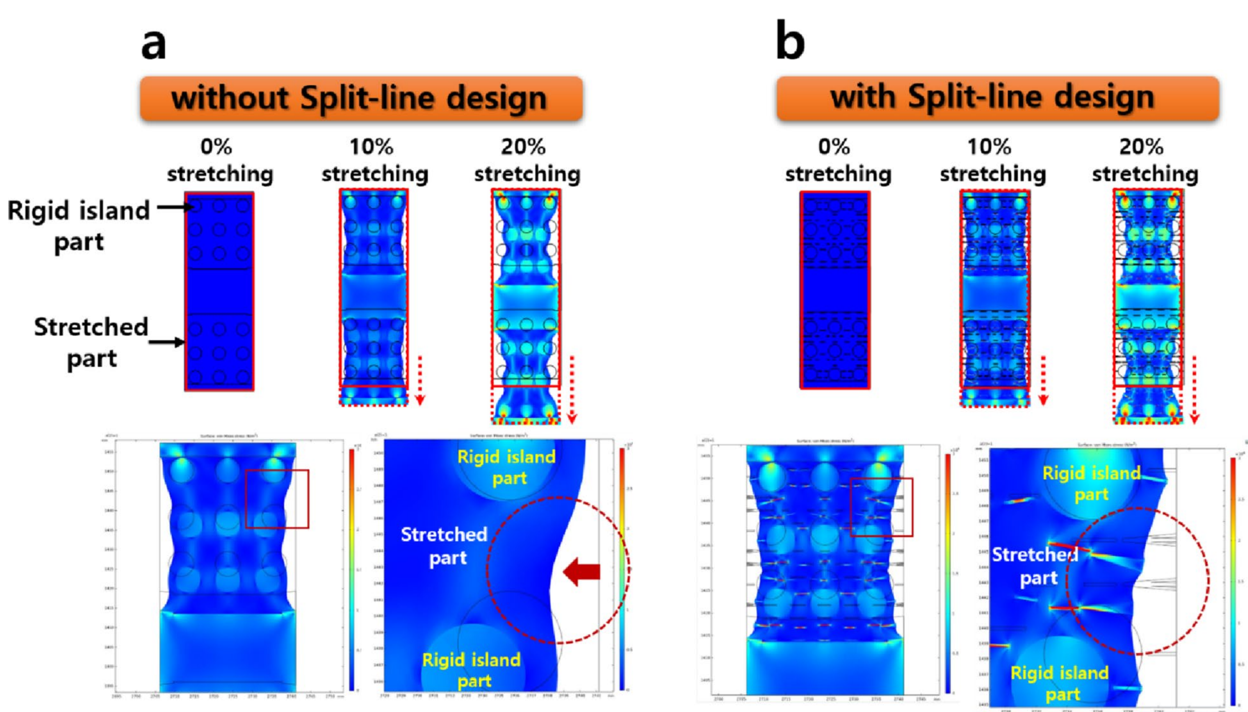

Fig. 3 Simulation results of slimming in stretchable substrates **a** without and **b** with split-line patterns. Without split-lines, pronounced slimming occurs between rigid islands under tensile strain, indicating severe local strain concentration in the elastomer region. In contrast, the incorporation of split-lines effectively mitigates slimming by redistributing strain through compliant paths, leading to a more uniform deformation and reduced failure risk

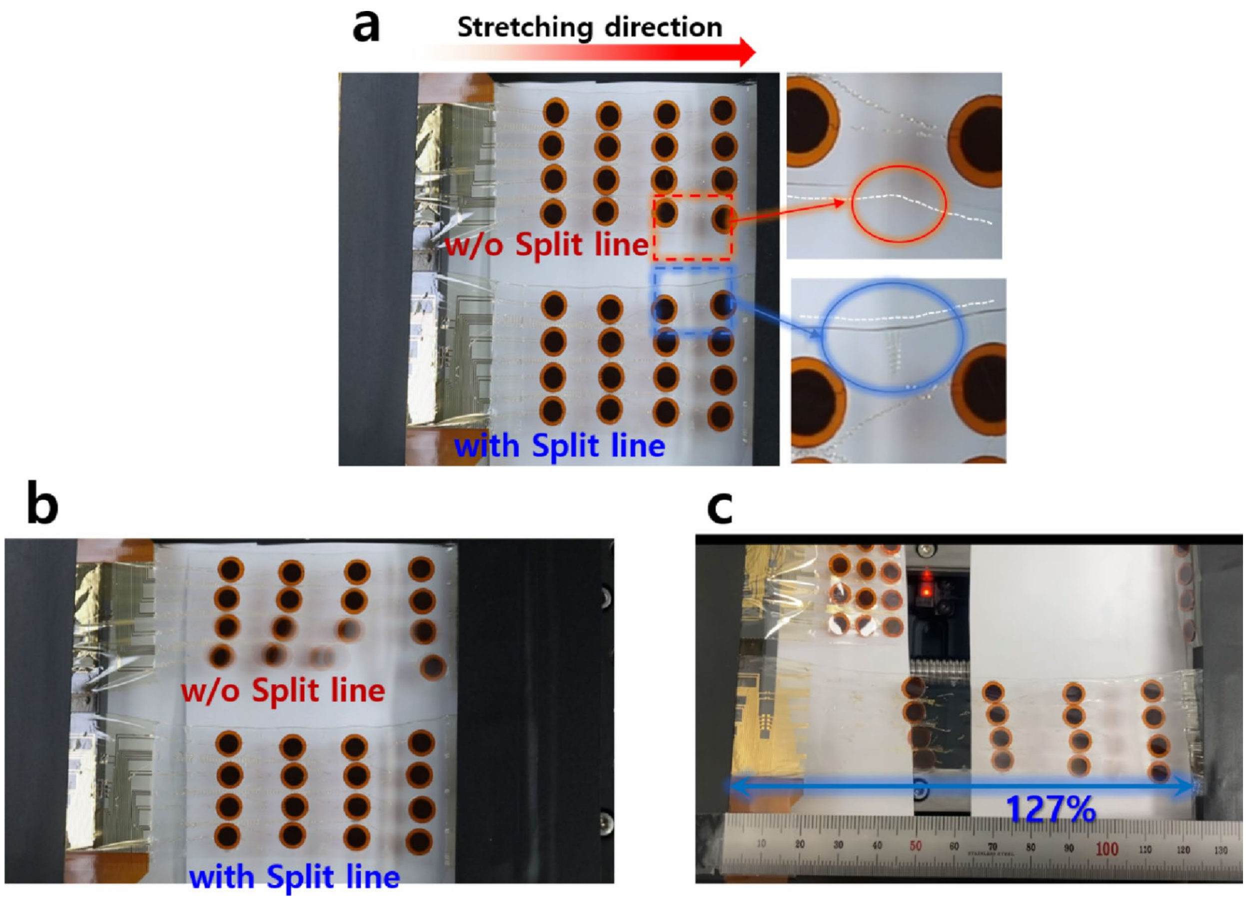

Fig. 4 Experimental comparison of stretch behavior with and without split-lines. **a** At 30% elongation, the region without split-lines exhibits pronounced slimming between rigid islands, whereas the split-line region maintains a uniform shape with suppressed necking. **b** At 35% elongation, cracks initiate and propagate in the no–split–line region, while the split-line design remains intact owing to effective strain redistribution. **c** The split-line patterned device endures up to 127% elongation without tearing, demonstrating over threefold enhancement in stretchability compared with the region lacking split-lines

stretching condition. The supplementary data clearly demonstrate that, while the region without split-lines exhibits severe slimming, the split-line-patterned region maintains uniform geometry without noticeable slimming. These visual comparisons reinforce that the split-line pattern effectively mitigates necking and distributes strain evenly during stretching.

Progressing to 35% elongation (Fig. 4b), the difference becomes decisive. The no–split-line section exhibits cracks nucleating precisely at the necked zones, leading to premature failure of the stretchable substrate. This deformation sequence is further visualized in Supplementary Figure S2, which shows that, in the absence of the split-line design, pronounced slimming first occurs at 30% strain, followed by crack initiation at 35%, and eventually results in substrate tearing and severe mechanical damage under continued elongation. These observations confirm that local strain accumulation in the narrow interconnect regions accelerates the onset of cracking and tearing, explaining the early mechanical failure of the device without split-lines. By comparison, the with–split-line section remains intact and maintains geometric integrity, corroborating that strain redistribution mitigates neck growth and delays crack initiation. Finally, Fig. 4c demonstrates a 127% elongation achieved by the split-line design without tearing. The result highlights a more than threefold improvement in attainable stretch relative to the failure limit (~35%) of otherwise identical regions lacking split-lines. Given that the only design modification is the insertion of simple split-line motifs, these findings underscore a minimal-complexity, layout-level strategy for markedly enhancing mechanical robustness and usable strain window in wafer-processed, multi-modal sensor platforms.

Pressure and bending sensor properties

Figure 5a presents the low-resolution 8-channel pressure sensor integrated on the stretchable substrate, where each sensing unit has an active-area diameter of 5.55 mm. The sensor adopts a laminated architecture in which an

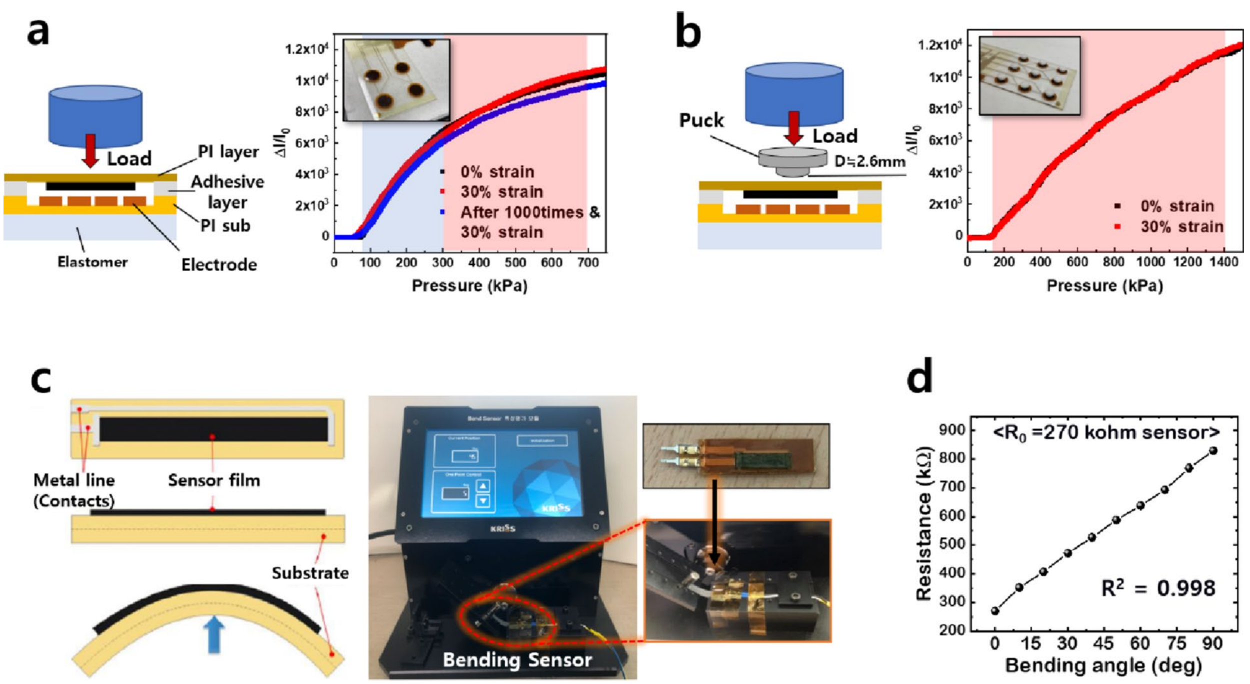

Fig. 5 Pressure and bending sensing characteristics on the stretchable platform. **a** Laminated IDE-based 8-channel pressure sensor: device architecture and pressure response at 0%/ 30% strain and after cyclic stretching; gain roll-off at higher pressures is attributed to partial closure of the sensing gap by the adhesive layer. **b** 18-channel array with an integrated 2.6-mm puck that concentrates contact force, preserving broad-range sensitivity even under 30% elongation—useful for firm robotic grasps. **c** Conductive-polymer bending sensor structure and measurement set-up with bending sensor. **d** Resistance–angle characteristics from 0–90° show near-linear behavior ($R^2 \approx 0.998$), enabling straightforward calibration for curvature estimation

interdigitated electrode (IDE) patterned on a polyimide (PI) substrate is laminated to an elastomer support; a thin adhesive layer bonds a top PI encapsulation ("PI layer") to the pressure-sensor sheet. This stacked structure provides mechanical compliance and packaging robustness while maintaining a well-defined sensing gap. In the working range of 80–300 kPa, the device exhibits a sensitivity of 30.6 kPa^{-1} under the unstrained condition, which slightly decreased to 27.5 kPa^{-1} at 30% strain. At higher loads (300–700 kPa), the sensitivity decreases to 8.7 kPa^{-1}, which we attribute to progressive closure of the nominal 100-μm gap between the IDE and the conductive polymer due to compression of the adhesive layer. As the gap approaches closure, the effective transduction area increases sublinearly and the response begins to saturate, yielding a lower incremental sensitivity. Durability testing over 10^3 cycles of 0–30% elongation demonstrates excellent stability. The sensitivity remains nearly constant, changing from 8.7 to 8.4 kPa^{-1} in the 300–700 kPa range, with minimal variation ratios (6.7% in 80–300 kPa and 2.9% in 300–700 kPa). These results indicate good stretch endurance of the laminated stack, with minimal signal drift under repeated deformation. Beyond sensitivity metrics, an explicit definition of the pressure–current input–output relation is essential for reproducible calibration and system-level deployment. To explicitly define the input–output (I/O) relation of the PU-based pressure sensor, we modeled the static mapping between the applied pressure P (kPa) and the baseline-corrected current change ΔI using a data-driven least-squares approach. After baseline correction ($\Delta I = I - I_0$) and restricting the analysis to the loading phase to mitigate hysteresis effects, the sensor response was well described by a piecewise linear model. Prior to cyclic stretching, the fitted relations yielded high coefficients of determination: $R^2 = 0.9858$ for 80–300 kPa and $R^2 = 0.9795$ for 300–700 kPa (0–700 kPa: $R^2 = 0.9710$). Importantly, the calibrated I/O characteristics remained comparable after 1000 stretch cycles, with consistently high goodness-of-fit ($R^2 \approx 0.97$–0.99) and only minor changes in sensitivity. In particular, the high-pressure-region slope (300–700 kPa) changed by approximately 2.4%, indicating that cyclic stretching does not significantly alter the pressure-to-current transfer relation of the PU-based sensor. These results provide an explicit, reproducible I/O definition for the sensing system and quantitatively demonstrate that the identified I/O relation is robust against repeated mechanical stretching. Figure 5b shows the photograph and pressure-sensing characteristics of the high-resolution 18-channel pressure sensor array designed for robotic gripper applications. Each individual sensing unit has a reduced diameter of 3.69 mm, enabling higher spatial resolution compared with the 8-channel array shown in Fig. 5a. To compensate for the smaller contact area and to ensure efficient force transfer during grasping, a circular polyurethane puck with a diameter of 2.6 mm was fabricated and positioned on top of each sensing element. This puck-assisted structure concentrates the applied load onto the active sensing region, thereby extending the measurable pressure range. The pressure response was evaluated over a wide range from 0 to 1500 kPa. Before substrate stretching, the sensor exhibited a sensitivity of 9.2 kPa^{-1} in the high-pressure regime of 140–1400 kPa. Notably, after 30% uniaxial stretching of the substrate, the sensitivity remained essentially unchanged at approximately 9.2 kPa^{-1}, demonstrating excellent mechanical robustness and stable pressure transduction under tensile deformation. Compared with the 8-channel array, the 18-channel configuration enables reliable detection of substantially higher pressures, which is particularly advantageous for firm grasping scenarios in robotic manipulation. Furthermore, the pressure-dependent sensitivity characteristics can be selectively utilized depending on the target robotic application, allowing optimization for either delicate touch sensing or high-force grasping. This tunable sensing behavior highlights the versatility of the proposed pressure sensor architecture for diverse robotic gripper use cases.

Figure 5c illustrates the device architecture and the test setup used to evaluate the bending sensor. Each bending sensor is an individual unit fabricated on a polyimide (PI) substrate and subsequently integrated onto the flexible–stretchable substrate via a flip-chip bonding process. On this integrated substrate, the bending sensor remains positioned on the top conductive pad on PI layer. Therefore, variations in interconnect resistance or geometric deformation during stretching are minimal, indicating negligible influence of substrate elongation on the bending-sensor characteristics. However, as the PI layer itself experiences tensile strain under stretching, monitoring possible structural or electrical changes at the flip-chip bonded interface becomes more critical for assessing the overall reliability of the integrated system. The right photograph of Fig. 5c shows the sensor mounted on a benchtop bending fixture for controlled angle sweeps (0°–90°), with electrical leads connected to the contact pads. Figure 5d reports the resistance response of a device with an initial resistance $R_0 \approx 270$ kΩ. As the bending angle increases from 0° to 90°, the resistance rises almost linearly, yielding a coefficient of determination $R^2 = 0.998$. As a result, the high linearity across two devices with different R_0 values, maintained without interfacial failure under tensile strain, indicates a robust strain transduction mechanism in the conductive-polymer layer and supports a simple linear calibration for bending angle estimation. Together with the verified operation of the temperature/humidity and proximity sensors, these results further substantiate that, when the multimodal sensor system is integrated on the top of the polyimide sheet through a chip bonding process on the proposed flexible and stretchable substrate, it exhibits high reliability and robust multimodal sensing capability.

Integration of temperature, humidity and proximity sensors for gripper applications

Figure 6a shows photographs of the solder paste printing and chip-bonding process for integrating sensor chips onto the stretchable substrate. The solder paste was screen-printed onto the electrode pads designed for the two different sensor types: the upper four pads correspond to the temperature/humidity sensor, and the lower eight pads correspond to the proximity sensor. Sensor chips were then aligned and bonded onto these pads using a reflow process to ensure mechanical stability and electrical continuity. Figure 6b presents the successful integration of sensor chips, clearly showing the bonded temperature/humidity and proximity sensor chips on the stretchable substrate.

The experimental setup for the robotic arm evaluation, including the placement of the proximity and temperature/humidity sensors, is shown in Fig. 6c. A robotic arm equipped with a target object was programmed to approach and retract from the proximity, temperature, and humidity sensors, while the corresponding environmental data were simultaneously monitored. Figure 6d shows the functional test results for both sensors. During testing, we positioned a black square, plate-shaped object directly in front of the sensor-equipped robotic arm. As the robotic arm approached the target plate, the proximity signal increased sharply, confirming accurate distance detection even through partial obstruction. Meanwhile, the temperature and humidity readings remained constant at ambient conditions (~ 26 °C and 47.2% RH), validating stable sensor baselines. Figure 6e demonstrates simultaneous measurement of proximity, temperature, and humidity signals during cyclic breathing tests conducted at a distance of approximately 5 cm. Each time breath was exhaled toward the sensor, a distinct proximity peak appeared as the face moved closer, accompanied by rapid increases in temperature (~ 30 °C) and humidity (~ 95%), followed by recovery to baseline. This synchronized variation across all three signals verifies that the multimodal sensing system operates reliably and responsively, capturing both environmental and positional dynamics. The results confirm that the system provides accurate proximity detection and rapid response to dynamic environmental stimuli such as temperature and humidity, demonstrating its robustness for real-time robotic and wearable applications that require multimodal sensing and perception.

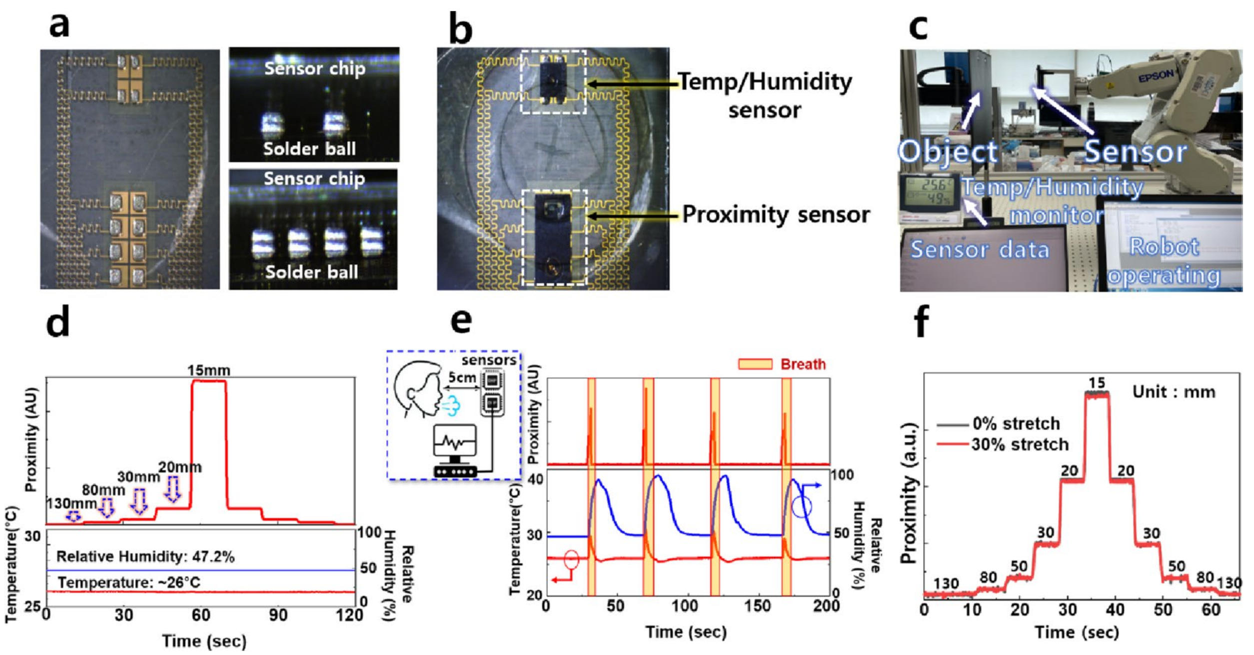

Fig. 6 Integration and functional validation of temperature/humidity and proximity sensors. **a** Screen-printed solder paste on designated electrode pads (upper: temperature/humidity, lower: proximity). **b** Flexible substrate with integrated sensor chips. **c** Experimental setup showing the robotic arm approaching the target object while sensor data are recorded in real time. The setup includes a proximity sensor and a temperature/humidity sensor for multimodal signal acquisition. **d** Proximity response to robotic arm approach, confirming accurate distance sensing through obstacles. **e** Simultaneous detection of proximity, temperature, and humidity variations during breathing, with synchronized signal peaks validating reliable multimodal operation. **f** Proximity sensor response before and after 30% stretching, demonstrating stable sensing performance and signal reliability under tensile deformation

As mentioned above, the bending sensor and the sensor chips (temperature/humidity and proximity) were mounted on metal pads formed on the polyimide layer, which remains undeformed during substrate stretching, using a flip-chip reflow bonding process. To evaluate potential issues such as detachment or performance degradation of the bonded chips under stretching, experiments were conducted using the bonded proximity sensor as a representative example. As shown in Fig. 6f, even after 30% elongation, the proximity sensor exhibited a signal variation of less than 2%, demonstrating stable performance and reliable operation under tensile deformation. These findings suggest that sensors integrated through the flip-chip reflow bonding process can maintain stable signal output even under mechanical stretching, confirming the robustness of the bonding interface and electrical interconnection. For robotic gripper applications, both multimodal sensing capability and operational reliability are essential to ensure precise perception and adaptive control. The integrated multimodal sensors on the flexible and stretchable substrate meet these requirements by providing stable signal outputs under mechanical deformation and consistent responses across multiple sensing modalities. Such performance is expected to enable more accurate object recognition, stable grasp control, and environmental adaptability in next-generation robotic systems.

Conclusions

In this work, a stretchable multimodal sensor platform was developed by employing a slimming-reduction (split-line) structural substrate, which significantly improved mechanical reliability and stretchability, achieving up to 127% elongation without fracture. This design effectively redistributed localized strain, thereby suppressing necking and crack propagation even under large tensile deformation. On this mechanically enhanced platform, various sensing components—including pressure, bending, temperature/humidity, and proximity sensors—were monolithically integrated. The pressure sensors maintained stable sensitivity (27–30 kPa^{-1} for 8-channel IDE type; 9.2 kPa^{-1} for 18-channel puck-assisted type) even after 30% stretching and 10^3 cyclic deformations, owing to negligible resistance variation (≤ 3.7%) in the serpentine interconnects. The bending sensor exhibited highly linear resistance–angle characteristics ($R^2 \approx 0.998$), and the environmental sensors reliably detected temperature, humidity, and proximity changes with rapid response. The flip-chip reflow bonding process provided strong electrical and mechanical connections between the sensor chips and the conductive pad on polyimide layer, maintaining stable performance even under mechanical stretching. The experimental results demonstrate the robustness of this integration approach, indicating that sensors fabricated through the same process can reliably preserve their signal integrity during deformation. Collectively, these results demonstrate a mechanically compliant yet functionally robust multimodal sensing system, providing a feasible route toward intelligent robotic grippers capable of adaptive and environment-aware manipulation. The proposed split-line strategy offers a low-complexity, wafer-compatible design approach for next-generation stretchable electronics and multifunctional e-skin platforms.

Supplementary Information

The online version contains supplementary material available at https://doi.org/10.1186/s40486-026-00263-7.

Supplementary Material 1.

Acknowledgements

This work was supported by Technology Innovation Program (Grant No. RS-2022-00154781, Development of large-area wafer-level flexible/stretchable hybrid sensor platform technology for formfactor-free highly integrated convergence sensor) funded By the Ministry of Trade, Industry & Energy (MOTIE, Korea).

Author contributions

C.-H. Hong conceived the overall concept and idea of the study, designed and fabricated the stretchable substrate, performed device characterization and analysis, and wrote the manuscript. S.-R. Seo contributed to the device fabrication and characterization. M.-S. Kim fabricated the pressure and bending sensors and conducted the bending-sensor measurements. M.-H. Kang and Y.-K. Hong were responsible for the integration and evaluation of the temperature/humidity and proximity sensors. H.-J. Kim supervised the entire project, provided strategic guidance on experimental design and data interpretation, and contributed to manuscript revision and finalization. All authors discussed the results and approved the final version of the manuscript.

Funding

This work was supported by the Korea Evaluation Institute of Industrial Technology (KEIT) grant funded by the Korea Government (MOTIE) (No. RS-2022-00154781, Development of large-area wafer-level flexible/stretchable hybrid sensor platform technology for formfactor-free highly integrated convergence sensor).

Data availability

The datasets used during the current study are available from the corresponding author on reasonable request.

Declarations

Competing interests

The authors declare no competing interests.

Author details

[1]Electronics and Telecommunications Research Institute, Daejeon, Korea
[2]Korea Research Institute of Standards and Science, Daejeon, Korea
[3]Korea Electronics Technology Institute, Jeonju, Korea
[4]University of Science and Technology, Daejeon, Korea

Received: 21 October 2025 / Accepted: 6 July 2026
Published online: 27 July 2026

References

1. Wang T, Li J, Zhang H et al (2024) Multimodal Sensors Enabled Autonomous Soft Robotic System with Self-Adaptive Manipulation. ACS Nano 18(14). https://doi.org/10.1021/acsnano.3c11281
2. Mao Q, Li X, Liu Y et al (2024) Multimodal tactile sensing fused with vision for dexterous manipulation. Nat Commun 15. https://doi.org/10.1038/s41467-024-51261-5
3. Hegde C, Culjat M, Wappett MA et al (2023) Sensing in Soft Robotics. ACS Nano 17(17). https://doi.org/10.1021/acsnano.3c04089
4. Zhang L, Xing S, Yin H et al (2024) Skin-inspired, sensory robots for electronic implants. Nat Commun 15:4777. https://doi.org/10.1038/s41467-024-48903-z
5. Qiu Y, Sun S, Wang X et al (2022) Nondestructive identification of softness via bioinspired multisensory electronic skin. npj Flex Electron 6:45. https://doi.org/10.1038/s41528-022-00181-9
6. Weiner P, Neef C, Shibata Y, Nakamura Y, Asfour T (2020) An Embedded, Multi-Modal Sensor System for Scalable Robotic and Prosthetic Hand Fingers. Sensors 20(1):101. https://doi.org/10.3390/s20010101
7. Abah C, Orekhov AL, Johnston GLH, Simaan N, Multi-Modal A (2022) Sensor Array for Human-Robot Interaction and Confined Spaces Exploration Using Continuum Robots. IEEE Sens J 22(4):3585–3596. https://doi.org/10.1109/JSEN.2021.3140002
8. Yu Y, Peng S, Sha Z, Cheng TX, Wu S, Wang CH (2021) High-precision, stretchable kirigami-capacitive sensor with minimized thermal–mechanical crosstalk. J Mater Chem A 9:24874–24886. https://doi.org/10.1039/D1TA06978K
9. Lee J-H, Chee P-S, Lim E-H, Low J-H, Nguyen N-T (2022) A Stretchable Kirigami-Inspired Self-Powered Sensor. Adv Eng Mater 24(4):2100961. https://doi.org/10.1002/adem.202100961
10. Kumaresan Y, Min G, Dahiya AS, Ejaz A, Shakthivel D, Dahiya R (2022) Kirigami and Mogul-Patterned Ultra-Stretchable High-Performance ZnO Nanowires-Based Photodetector. Adv Mater Technol 7(1):2100804. https://doi.org/10.1002/admt.202100804
11. Sun F, Lu Q, Feng S, Zhang T (2021) Flexible Artificial Sensory Systems Based on Neuromorphic Devices. ACS Nano 15(3):3875–3899. https://doi.org/10.1021/acsnano.0c10049
12. Li J, Wang H, Zhang C et al (2024) Design of AI-Enhanced and Hardware-Supported Multimodal E-Skin for Environmental Object Recognition and Wireless Toxic Gas Alarm. Nano-Micro Lett 16:256. https://doi.org/10.1007/s40820-024-01466-6
13. Editorial (2022) A soft touch for robots. Nat Mach Intell 4:607–608. https://doi.org/10.1038/s42256-022-00496-2
14. Park H, Cha Y (2025) Liquid classification in robotic fingers with multimodal tactile sensing. npj Rob 3:51. https://doi.org/10.1038/s44182-025-00051-2
15. Zhang N, Ren J, Dong Y et al (2025) Soft robotic hand with tactile palm–finger coordination. Nat Commun 16:2395. https://doi.org/10.1038/s41467-025-57741-6
16. Jung J, Lee S, Kim H et al (2024) Self-healing electronic skin with high fracture strength and toughness. Nat Commun 15:7392. https://doi.org/10.1038/s41467-024-53957-0
17. Vo NTP, Nam TU, Jeong MW et al (2024) Autonomous self-healing supramolecular polymer transistors for skin electronics. Nat Commun 15:3433. https://doi.org/10.1038/s41467-024-47718-2
18. Xu Y, Sun Z, Bai Z et al (2024) Bionic e-skin with precise multi-directional droplet sliding sensing for enhanced robotic perception. Nat Commun 15:6022. https://doi.org/10.1038/s41467-024-50270-8
19. Ye L, Wang Z, Li H et al (2025) A flexible self-powered multimodal sensor with low cross-sensitivity. Chem Eng J 519:164866. https://doi.org/10.1016/j.cej.2025.164866
20. Cao VA, Phan QV, Khanh NN, Kim M (2025) Multifunctional tactile sensor with multimodal capabilities for pressure/temperature/texture detection. Mater Today Phys 40:101599. https://doi.org/10.1016/j.mtphys.2025.101599
21. Sreevanya GV, Lee S-J, Cheon H, Kim M, Kim HK (2024) Highly stretchable and flexible kirigami-patterned silver electrodes for wearable electronics. Compos Part B: Eng 276:111052. https://doi.org/10.1016/j.compositesb.2024.111052
22. Choi JC, Chung S et al (2024) Bidirectional Zero Poisson's Ratio Elastomers with Self-Deformable Soft Mechanical Metamaterials for Stretchable Displays. Adv Funct Mater 34:2406725. https://doi.org/10.1002/adfm.202406725

23. Keum K, Yang S, Kim KS, Park S-K, Kim Y-H (2024) Recent progress of stretchable displays: a comprehensive review. Soft Sci 4(4):34. https://doi.org/10.20517/ss.2024.26

Publisher's Note